Journal of Rubber Research (2020) 23:287–299
https://doi.org/10.1007/s42464-020-00057-5

ORIGINAL PAPER

A framework for model base hyper-elastic material simulation

Amirheshmat Khedmati Bazkiaei[1] · Kourosh Heidari Shirazi[1] · Mohammad Shishesaz[1]

Received: 26 February 2020 / Accepted: 16 September 2020 / Published online: 8 October 2020

Abstract
In this research, a framework for modelling and simulation of hyper-elastic materials is proposed. The framework explains how to employ strain energy functions as a constitutive model, standard loading test data, and a powerful optimisation method to determine a mathematical function for explaining the mechanical behaviour of a hyper-elastic material using minimum types of loading test data. In the first part, a survey on hyper-elastic constitutive models is presented. Fifty models are collected and classified into six categories. Thereafter, five types of standard loading tests including uniaxial, biaxial, equi-biaxial, pure shear, and simple shear are introduced. It is shown that depending on the loading type, physical parameters, Cauchy, and nominal stress tensors, each constitutive model possesses a particular function. The genetic algorithm as a powerful optimisation method is used to determine the most accurate function for each type of loading test data. It is presented that based on the selected constitutive model and regardless of a number of existing loading types test data, a unique function can be determined for expressing and simulating the mechanical behaviour of the considered hyper-elastic material.

Keywords Hyper-elastic models · Genetic algorithm · Constitutive model · Mooney–Rivlin · Ogden

Abbreviations

w	Stored strain energy function
S_{ij}	Piolla–Kirchhof second stress tensor components
E_{ij}	Green–Lagrange strain tensor components
C_{ij}	Right Cauchy-Green deformation tensor components
δ_{ij}	Kronecker delta
F_{ij}	Deformation gradient tensor components
X_i	Non-deformed body
U_i	Displacement field
λ_i^2	Eigenvalues of right Cauchy–Green tensor
λ_i	Eigenvalues of deformation gradient tensor
J	Jacobian
I_i	Invariants of Cauchy-Green strain tensor
H_{ij}	Components of Hessian matrix of stored energy function
C_{pq}	Model parameters
α_i	Model parameters
μ_i	Model parameters
I_m	Limiting value of 1st invariant
J_m	Parameter of finite chain extensibility
μ	Model parameters
n	Chain density per unit of volume
k	Boltzman constant
T	Absolute temperature
$\mathcal{L}^{-1}$	Langevin function
$I^*(\alpha)$	First invariant of the generalised α-order strain tensor
B_i	Model parameters
A_i	Model parameters
P	Nominal stress
p	Hydrostatic pressure

Introduction

Rubbers are categorised among nonlinear elastic or hyper-elastic materials. The molecular structure of hyper-elastic materials permits high flexibility in room temperature as well as high reversibility against deformation. The most important property of these materials is incompressibility, which is the reason for having Poisson's ratio near 0.5. This causes the complexity of numerical calculations, especially in three-dimensional analysis. The unique properties of these materials make them highly applicable in everyday life and science. In addition to the wide application of these materials in the automotive industry, aerospace, and tires [1–5],

✉ Kourosh Heidari Shirazi
k.shirazi@scu.ac.ir

[1] Department of Mechanical Engineering, Shahid Chamran University of Ahvaz, Ahvaz 61357-43337, Iran

railway industry [6–8], power devices and motors [9], and bearings [10], this kind of materials also are used in medical sciences. Investigations on heart muscles [11–16], tendon and ligaments under different loads [17–20], body skin under special circumstances like injections [21–26], brain tissues' behaviour [27–32], cancer cure and the spread of cancer inside human body [33–35], rehabilitation of disabled or diabetic patients [36, 37] are some of these applications. Another highly applicable field for these materials is sports sciences. Other applications of the hyper-elastic material include their vast usage in sports' instruments like clothing [38–40], basketball, baseball and golf balls [41, 42] and sports tracks [43] as well as injuries due to impact of the ball and other hyper-elastic materials to the human body in sports matches [44–50].

It is known that the mechanical properties of materials are defined by their response to the environment and circumstances loads. To investigate the mechanical properties, some experiments should be designed. The results of the experiments usually are in the form of diagrams and tables e.g. stress–strain diagrams. Unlike free energy models such as Helmholtz free energy function and Gibbs function in the constitutive models of hyper-elastic materials, the mechanical behaviour of rubber-like materials, some polymers, foams, and so on are expressed in terms of strain energy in isotropic, incompressible and constant temperature conditions. In elastic materials, stress tensor is obtained with the derivation of the strain energy density function with respect to the strain; however, for hyper-elastic material stress tensor, the derivation of the strain energy function should be performed with respect to deformation gradient tensor due to large deformation. In recent decades, several functions are introduced as the strain energy density function. In 1940, Mooney [51] introduced one of the most significant models of hyper-elastic materials. This model is defined based on the linear response of rubber under simple shear loads. In 1942, strain energy function for a single chaincase was found, using non-Gaussian assumption in the limiting extensibility of polymer chains [52]. In 1943, another model was introduced using molecular networks and static Gaussian law by Treloar [53]. Rivlin and Saunders [54] established standard experiments that led to discovering some new facts about the deformation of hyper-elastic materials. Later on, Isihara et.al [55] used the result data of Rivlin and Saunders experiment as reference data. Some novel models were introduced for strain energy function to investigate spherical membranes in 1966 [56], soft body tissues in 1967 [57], interactions between the balloon and its fluid with respect to height change in 1968 [58]. In 1981 [59], a novel model was introduced to express the mechanical properties of hyper-elastic based on network chains assuming their slide on their connections. Another model has presented under the assumption of real network chains general theory and restriction of movements of connection points between network chains and another adjacent in 1982 [60]. Considering Van der Waals forces and assuming gas behaviour for rubber network under influence of forces between quasi-particles, a novel model was introduced in 1986 [61]. The existence and behaviour of cracks in hyper-elastic materials were investigated in 1997 [62]. In 2000, stress was expressed in terms of guessed functions [63]. Later on, some other models were introduced which are a combination between previous models such as [64, 65], novel systematic experiments [66], and models sensitive to certain experiments [67].

In the present work, in Sect. 2, a discussion and classification on strain energy functions are performed. In Sect. 3 based on the introducing five standard loading physical constants, Cauchy stress tensor, hydrostatic pressure, and nominal stress tensor are obtained. In Sect. 4, the genetic algorithm (GA) method (one of the meta-heuristics that has been employed to find optimum solution of many combinational problems [68–70]) is discussed for optimal parameters and function estimation. In the final section, concluding remarks are presented.

Stored strain energy

As was mentioned before, in hyper-elastic materials, the stress tensor is defined as a derivative of stored energy function concerning the deformation gradient. This can be written in the form of the following equation:

$$S_{ij} = \frac{\partial \mathrm{w}}{\partial E_{ij}} = 2\frac{\partial \mathrm{w}}{\partial C_{ij}}, \qquad E_{ij} = \frac{1}{2}\left(C_{ij} - \delta_{ij}\right), \tag{1}$$

where, S_{ij} is Piolla–Kirchhof second stress tensor components, w is stored strain energy function, E_{ij} is Green–Lagrange strain tensor components, C_{ij} is right Cauchy–Green deformation tensor components and δ_{ij} is Kronecker delta. Right Cauchy–Green deformation tensor is defined as a function of deformability gradient tensor, which is expressed in Eq. 2:

$$C_{ij} = F_{ik}F_{kj}, \qquad F_{ik} = \frac{\partial \mathrm{x_i}}{\partial \mathrm{X_k}}, \tag{2}$$

where F_{ij} is deformation gradient components, X_i is non-deformed body, $x_i = X_i + U_i$ is deformed body and U_i is displacement field. Eigenvalues of C_{ij} exist, if and only if

$$\det\left(C_{ij} - \lambda_{\mathrm{p}}^2\delta_{ij}\right) = 0, \tag{3}$$

from the characteristic equation

$$\lambda_p^6 - I_2\lambda_p^4 + I_2\lambda_p^2 - I_3 = 0, \tag{4}$$

where

$$\begin{aligned} I_1 &= tr(C) = \left(\lambda_1\right)^2 + \left(\lambda_2\right)^2 + \left(\lambda_3\right)^2, \\ I_2 &= \frac{1}{2}\left\{(\mathrm{tr}C)^2 - tr\left(C^2\right)\right\} = \left(\lambda_1\lambda_2\right)^2 + \left(\lambda_1\lambda_3\right)^2 + \left(\lambda_2\lambda_3\right)^2, \\ I_3 &= \left(\lambda_1\lambda_2\lambda_3\right)^2 = J^2, J = \det\left[F_{ik}\right]. \end{aligned} \tag{5}$$

The third invariant is not commonly used for these sorts of models, because it signifies the constant volume or Poisson's ratio ~ 0.5. Where $\lambda_i{}^2$ are eigenvalues of right Cauchy–Green tensor and λ_i are eigenvalues of deformation gradient tensor, J (Jacobian) is the ratio of deformed elastic volume to initial volume of the material. In these materials, the determinant of the deformation gradient is equal to unity. Therefore, stored energy function, which depends on deformations and is not depended on rigid body movements, is expressed in terms of first and second invariants as follows:

$$w = w\left(I_1(C), I_2(C)\right). \tag{6}$$

These energy functions have to satisfy some essential conditions, which are

absence of energy, if there is no deformation

$$w_{\mathrm{un}} = 0. \tag{7}$$

The amount of energy and the resulting stress is infinite for huge deformations

$$\begin{aligned} &\lim_{\lambda_i\to\infty} \mathrm{w} = +\infty \qquad \lim_{\lambda_i\to 0} \mathrm{w} = +\infty, \\ &\lim_{\lambda_i\to\infty} \frac{\partial \mathrm{w}}{\partial\lambda_i} = +\infty \qquad \lim_{\lambda_i\to 0} \frac{\partial \mathrm{w}}{\partial\lambda_i} = -\infty. \end{aligned} \tag{8}$$

Absence of stress, if there is no deformation; and its amount has to be minimum

$$\begin{aligned} &\frac{\partial w}{\partial\lambda_i}|_{\lambda_1=\lambda_2=\lambda_3=1} = 0 \qquad \frac{\partial^2 w}{\partial\lambda_i^2}|_{\lambda_1=\lambda_2=\lambda_3=1} > 0. \\ &\det\left[H_{ij}\right] > 0, H_{ij} = \frac{\partial^2 w}{\partial\lambda_i\partial\lambda_j}|_{\lambda_1=\lambda_2=\lambda_3=1}, i,j \in \{1,2,3\}, \end{aligned} \tag{9}$$

where H_{ij} are the components of the Hessian matrix of the stored energy function, without any deformations. Generally, there are two principles to construct stored energy function as a model of hyper-elastic.

The first principle uses the Rivlin series [68] with a known number of parameters or Ogden expansion [69, 70]. For incompressible materials, Rivlin series is described as

$$w_{\mathrm{Ri}} = \sum_{p,q=0}^{\infty} C_{pq}\left(I_1 - 3\right)^p\left(I_2 - 3\right)^q. \tag{10}$$

And Ogden expansion as

$$w_{\mathrm{Og}} = \sum_{p=1}^{\infty} \frac{\mu_p}{\alpha_p}\left(\lambda_1^{\alpha_p} + \lambda_2^{\alpha_p} + \lambda_3^{\alpha_p} - 3\right), \tag{11}$$

where C_{pq}, μ_p and α_p are material characteristics, under condition $C_{00} = 0$.

In the second principle, which is essential for modelling based on experimental data, $\partial w/\partial I_1$ is independent of I_1 and I_2 for low values and dependent on I_1 for high values and $\partial w/\partial I_2$ is independent of I_1 but a descending function of I_1.

Various stored strain energy models can be categorised in the following section.

Models based on first and second invariants

Polynomial function of first invariant

Although in these models, the effect of the second invariant is neglected, they have no valid predictions for some kinds of deformation. Moreover, they show poor results for shear and biaxial stress. These models are listed in Table1.

Polynomial function of first and second invariants

These models use the following function:

$$w_{I_1-I_2-\mathrm{based}} = \sum_{p=1}^{\infty} \frac{C_{p0}}{p}\left(I_1 - 3\right)^p + \sum_{q=1}^{\infty} \frac{C_{0q}}{q}\left(I_2 - 3\right)^q. \tag{12}$$

Most of these models use the Mooney–Rivlin model's expansion. Their prediction for biaxial deformation modes is poor. Generally speaking, models that have the term $(I_2 - 3)^q$ for $q \geq 1$ are not accurate for biaxial results. In Table 2 some of these models are presented.

Table 1 List of polynomial function of first invariant

Model	Equation	Years
Neo-Hookean	$w = \frac{\mu}{2}\left(I_1 - 3\right)$	1943 [53]
Rivlin	$w = \sum_{\mathrm{p=1}}^{\infty} \frac{C_{p0}}{p}\left(I_1 - 3\right)^p$	1948 [71]
Yeoh	$w = \sum_{\mathrm{i=1}}^{N} C_{\mathrm{i0}}\left(I_1 - 3\right)^i$	1990 [74]
Arruda–Boyce	$w = \mu\sum_{i=1}^{5} \frac{C_i}{\left(\lambda_m^{2i-2}\right)}\left[I_1^i - 3^i\right]$	1993 [75]
Yamashita–Kawataba	$w = C_{10}\left(I_1 - 3\right) + C_{N0}\left(I_1 - 3\right)^N$	1993 [76]
Gent	$w = -\frac{\mu J_m}{2}\ln\left(1 - \frac{I_1-3}{J_m}\right)$	1995 [77]
Oscar Lopez–Pamies	$w = \sum_{r=1}^{M} \frac{3^{1-\alpha_r}}{2\alpha_r}\mu_r\left(I_1^{\alpha_r} - 3^{\alpha_r}\right)$	2010 [78]
Hesebeck-Wulf	$w = \frac{A}{B\left(1-\exp\left(-B\left(I_1-3\right)\right)\right)} + \sum_{i=1}^{3} C_{i0}\left(I_1 - 3\right)^i$	2018 [79]

Function models with respect of first and second invariants

Generally, in this model, the following function is used:

$$w_{I_1-I_2-\text{based}} = f(I_1) + g(I_2). \tag{13}$$

In the function with respect to the second invariant, it is important to mention that $\partial g/\partial I_2$ is a positive function with respect to the second invariant and has a descending value. This is why logarithmic functions are used to express these functions. These functions are the resultants of power expansion of $I_2 - 3$ with a bounded convergence radius. The first invariant function is expressed in several forms; power series, exponential function: this function can be the result of Taylor series expansion with unbounded convergence radius, mirror function; in this function, the reflection of function $y(x) = 1/(a-x)^n$ is used to express $\partial w/\partial I_1$. Projection of this function is the reflection of $z(x) = 1/x^n$, functions y and z are symmetric with respect to $x = a/2$ and also x = a is the asymptotic value of y. This value can be introduced as limiting value for function with respect to the first invariant.

Some of these models are summarised in Table 3.

Model based on principal tensions of deformation gradient tensor

In these models, the focus is on eigenvalues of deformation gradient tensor. Mainly, Ogden expansion is used in these models which are listed in Table 4.

Models based on combinations of principal tensions of deformation gradient tensor and first and second invariants

In previous models, the focus was on constructing the functions, based on invariants or principal tensions only. It is possible to construct a function to express the behaviour of these materials, based on both of them. The list of these models is presented in Table 5.

Models based on chemical structures and quasi-rubber material network

This type of modelling focuses on the microscopic response of polymer chains in the material network. The process and instructions for making these materials play the main role in these models. The mechanical behaviour of quasi-rubbers is influenced by entropy changes that depend on molecular chain networks. In Table 6 a list of these models is presented.

Table 2 List of polynomial function of first and second invariants

Model	Equation	Year
Mooney-Rivlin	$w = C_{10}(I_1-3) + C_{01}(I_2-3)$	
	$\mathrm{w} = \mathrm{C}_{10}(\mathrm{I}_1-3) + \mathrm{C}_{01}(\mathrm{I}_2-3) + \mathrm{C}_{11}(\mathrm{I}_1-3)(\mathrm{I}_2-3)$	
	$w = C_{10}(I_1-3) + C_{01}(I_2-3) + C_{11}(I_1-3)(I_2-3) + C_{20}(I_1-3)^2 + C_{02}(I_2-3)^2$	1948 [51]
	$w = C_{10}(I_1-3) + C_{01}(I_2-3) + C_{11}(I_1-3)(I_2-3) + C_{20}(I_1-3)^2 + C_{02}(I_2-3)^2 + C_{21}(I_1-3)^2 + C_{12}(I_2-3)^2(I_1-3) + C_{30}(I_1-3)^3 + C_{03}(I_2-3)^3$	
Isihara	$w = C_{10}(I_1-3) + C_{01}(I_2-3) + C_{20}(I_1-3)^2$	1951 [55]
Bidermann	$w = C_{10}(I_1-3) + \frac{C_{20}}{2}(I_1-3)^2 + \frac{C_{30}}{2}(I_1-3)^2 + C_{01}(I_2-3)$	1958 [80]
Tschoegl	$w = C_{10}(I_1-3) + C_{01}(I_2-3) + C_{20}(I_1-3)^2 + C_{11}(I_1-3)(I_2-3) + C_{30}(I_1-3)^3$	1971 [81]
James et. al	$w = C_{10}(I_1-3) + C_{11}(I_1-3)(I_2-3) + C_{20}(I_1-3)^2 + C_{30}(I_1-3)^3 + C_{01}(I_2-3)$	1975 [82]
Swanson	$w = \frac{3}{2}\sum_{i=1}^{n}\frac{A_i}{1+\alpha_i}\left(\frac{I_1}{3}\right)^{1+\alpha_i} + \frac{3}{2}\sum_{i=1}^{n}\frac{B_i}{1+\beta_i}\left(\frac{I_2}{3}\right)^{1+\beta_i}$	1985 [83]
Lion	$w = C_{10}(I_1-3) + C_{01}(I_2-3) + C_{50}(I_1-3)^5$	1997 [84]
Haupt-Sedlan	$w = C_{10}(I_1-3) + C_{11}(I_1-3)(I_2-3) + C_{30}(I_1-3)^3 + C_{02}(I_2-3)^2 + C_{01}(I_2-3)$	2000 [85]
Beda	$w = \frac{C_1}{\alpha}(I_1-3)^{\alpha} + C_2(I_1-3) + \frac{C_3}{\beta}(I_1-3)^{\beta} + \frac{K}{\gamma}(I_2-3)^{\gamma}$	2005 [86]
Amin et.al	$w = C_{10}(I_1-3) + C_{(N+1)0}(I_1-3)^{N+1} + C_{(M+1)0}(I_1-3)^{M+1} + C_{01}(I_2-3)$	2006 [87]
Nunes	$w = C_1(I_1-3) + \frac{4}{3}C_2(I_2-3)^{3/4}$	2010 [66]
Carroll	$w = aI_1 + bI_1^4 + cI_2^{0.5}$	2011 [88]

Table 3 List of models based on function of first and second invariants

Model	Equation	Year
Rivlin–Saundres	$w = C(I_1 - 3) + f(I_2 - 3)$	1950 [54]
Gent–Thomas	$w = C_1(I_1 - 3) + C_2 ln\frac{I_2}{3}$	1958 [89]
Hart–Smith	$w = C\int e^{\beta(I_1-3)^2} dI_1 + Kln\frac{I_2}{3}$	1966 [56]
Fung	$w = C(e^{\beta(I_1-3)} - 1)$	1967 [57]
Alexander	$w = C_1\int e^{\beta(I_1-3)^2} dI_1 + C_2 ln\frac{I_2-3+\gamma}{\gamma} + C_3(I_2 - 3)$	1968 [58]
Veronda–Westmann	$w = C_1\left(e^{\beta(I_1-3)} - 1\right) - C_2(I_2 - 3)$	1970 [90]
Takamizawa–Hayashi	$w = -Cln(1 - \left(\frac{I_1-3}{I_m-3}\right)^2)$	1987 [91]
Holmes-Mow	$w = C_0\left[exp\left(C_1(I_1 - 3) + C_2(I_2 - 3)\right) - 1\right]$	1990 [92]
Yeoh-Fleming	$w = \frac{A}{B}\left(I_m - e^{-BR}\right) - C_{10}(I_m - 3)ln(1 - R)$	1997 [93]
Lambert-Diani-Rey	$w = C\int exp(\sum_{p=0}^{N} a_p(I_1 - 3)^p)dI_1 + \int exp(\sum_{p=0}^{N} b_p(lnI_2)^p)dI_2$	1999 [94]
Pucci-Saccomandi	$w = Kln\frac{I_2}{3} - \frac{\mu}{2}(I_m - 3)ln(1 - \frac{I_1-3}{I_m-3})$	2002 [64]
Beda	$w = \sum_{p=1}^{N} \frac{C_{p0}}{p}(I_1 - 3)^p + Kln\frac{I_2}{3}$	2007 [95]
Khajehsaeid et.al	$w = A[\frac{1}{a}exp\left(a(I_1 - 3)\right) + b(I_1 - 2)(1 - ln(I_1 - 2)) - \frac{1}{a} - b]$	2013 [67]

Table 4 List of models based on principal tensions of deformation gradient tensor

Model	Equation	Year
Valanis-Landel	$w = 2\mu\sum_{i=1,2,3}(\lambda_i(ln\lambda_i - 1))$	1967 [96]
Ogden	$w = \sum_{i=1}^{N} \frac{2\mu_i}{\alpha_i}(\lambda_1^{\alpha_i} + \lambda_2^{\alpha_i} + \lambda_3^{\alpha_i} - 3)$	1972 [72]
Peng-Landel	$w = \sum_{i=1,2,3} C[\lambda_i + \left(ln\lambda_i - 1\right) - \frac{(ln\lambda_i)^2}{6} + \frac{(ln\lambda_i)^3}{18} - \frac{(ln\lambda_i)^4}{216}]$	1972 [97]
Tobisch	$\frac{dw(\lambda_i)}{d\lambda_i} = 2\,\bar{G}\,exp(A(\lambda_i^2 - 1)) - B\lambda_i^{-3}$	1980 [98]
Shariff	$\sigma_i = -p + \lambda_i\frac{\partial w}{\partial\lambda_i} = f(\lambda_i)$ $f(\lambda) = E\sum_{j=0}^{n}\alpha_j\varphi_j(\lambda)$ $\alpha_0 = 1 \rightarrow \varphi_0(\lambda) = \frac{2ln(\lambda)}{3}$ $\varphi_1(\lambda) = e^{1-\lambda} + \lambda - 2, \varphi_2(\lambda) = e^{\lambda-1} - \lambda$ $\varphi_3(\lambda) = \frac{(\lambda-1)^3}{\lambda^{3.6}}, \varphi_j(\lambda) = (\lambda - 1)^j, j = 4,5,\ldots,n$	2000 [63]

Table 5 List of models based on combination of principal tensions and invariants

Model	Equation	Year
Gao	$w = a[(\lambda_1^2 + \lambda_2^2 + \lambda_3^2)^n + (\lambda_1^{-2} + \lambda_2^{-2} + \lambda_3^{-2})^n]$	1997 [62]
Beda-Chevalier	$w = K_1(I_1 - 3) + K_2 ln\frac{I_2}{3} + \frac{\mu}{\alpha}(\lambda_1^{\alpha} + \lambda_2^{\alpha} + \lambda_3^{\alpha} - 3)$	2003 [65]
Hessebeck-Wulf	$w = \frac{2\mu}{\alpha^2}\left(\lambda_1^{\alpha} + \lambda_2^{\alpha} + \lambda_3^{\alpha} - 3\right) + \frac{K}{2}(J - 1)^2$	2018 [79]
Narooei-Arman	$w = \sum_{i=1}^{\infty} A_i\left[exp\left(m_i\left(\lambda_1^{\alpha_i} + \lambda_2^{\alpha_i} + \lambda_3^{\alpha_i} - 3\right)\right) - 1\right]$ $+ \sum_{i=1}^{\infty} B_i\left[exp\left(n_i\left(\lambda_1^{-\beta_i} + \lambda_2^{-\beta_i} + \lambda_3^{-\beta_i} - 3\right)\right) - 1\right] + \frac{1}{K}(J - 1)^2$	2018 [99]

Physical parameter calculations of models

As it was shown before, strain energy functions have some parameters depending on natural parameters of materials. Finding these parameters causes the model to be able to express the mechanical behaviour of the rubber [102, 103]. In high strains hyper-elasticity, two stress tensors are introduced: true stress tensor (Cauchy) and nominal stress tensor (Piolla–Kirchhof first stress). In these materials, Cauchy stress tensor depends on the strain and an arbitrary parameter which is calculated from equilibrium equations. This parameter is called hydrostatic pressure, the unknown pressure in reaction to incompressibility constant, such that

$$\sigma_i = -p + \lambda_i\left(\frac{\partial w}{\partial I_1}\frac{\partial I_1}{\partial\lambda_i} + \frac{\partial w}{\partial I_2}\frac{\partial I_2}{\partial\lambda_i}\right) \tag{14}$$

Table 6 List of models based on chemical structures

Model	Equation	Year
3-chain	$w = nkT\left[\frac{\lambda}{\sqrt{N}}\mathcal{L}^{-1}\left(\frac{\lambda}{\sqrt{N}}\right) + ln\left(\frac{\mathcal{L}^{-1}\left(\frac{\lambda}{\sqrt{N}}\right)}{\sinh\left(\mathcal{L}^{-1}\left(\frac{\lambda}{\sqrt{N}}\right)\right)}\right)\right]$ $\rightarrow \frac{1}{2}nkT = \mu,$	1942 [52]
Treloar	$w = \frac{1}{2}nkT(I_1 - 3)$	1943 [53]
Slip-link	$w = \frac{1}{2}kTN_c\sum_{i=1}^{3}\lambda_i^2 + \frac{1}{2}kTN_s\sum_{i=1}^{3}\left[\frac{(1+\eta)\lambda_i^2}{1+\eta\lambda_i^2} + \ln\left\lvert 1+\eta\lambda_i^2\right\rvert\right]$	1981 [59]
Constrained junction	$w = \frac{1}{2}nkT\left(I_1 - 3\right) + \frac{1}{2}kT\mu\sum_{i=1}^{3}[k^2(\lambda_i^2-1)\left(\lambda_i^2+k\right)^{-2} + \lambda_i^2k^{-1}B_i - \ln\left(k^2(\lambda_i^2-1)(\lambda_i^2+k)^{-2}+1\right) - \ln(\lambda_i^2k^{-1}B_i+1)]$	1982 [60]
Van der waals	$G\{-\left(\lambda_m^2-3\right)\left[\ln\left(1-\sqrt{\frac{\beta I_1+(1-\beta)I_2-3}{\lambda_m^2-3}}\right) + \sqrt{\frac{\beta I_1+(1-\beta)I_2-3}{\lambda_m^2-3}}\right] - \frac{2}{3}(\frac{\beta I_1+(1-\beta)I_2-3}{2})^{\frac{3}{2}}\}$	1986 [61]
8-chain	$\sigma_i = \frac{nkT\sqrt{N}}{3}\frac{\lambda_i^2}{\sqrt{\frac{I_1}{3}}}\mathcal{L}^{-1}(\frac{\sqrt{\frac{I_1}{3}}}{\sqrt{N}})$	1993 [76]
Tube	$w = G_sI^*(2) - \frac{2G_e}{\beta}I^*(\beta)$	1997 [100]
Extended-tube	$w = G_sI^*(2) - \frac{2G_e}{\beta}I^*(\beta) + \frac{G_s}{2}[\frac{(1-\delta^2)(I_1-3)}{1-\delta^2(I_1-3)} + \ln(1-\delta^2(I_1-3))]$	1999 [101]

And nominal stress is given as follows:

$$P_i = -\frac{1}{\lambda_i}p + \frac{\partial w}{\partial I_1}\frac{\partial I_1}{\partial \lambda_i} + \frac{\partial w}{\partial I_2}\frac{\partial I_2}{\partial \lambda_i}. \tag{15}$$

To find these parameters, some experiments are required through which the strain is measured as a function of input forces. By curve fitting, the stored energy function on experimental results, the unknown parameters are taken into account. Different types of usual loadings, in which the strain energy function is used to express hyper-elastics' behaviour are uniaxial [104–107], equi-biaxial, pure shear, and biaxial loading [108]. The deformation gradient for each type of loading is as follows:

For equi-axial loading

$$\boldsymbol{F} = \begin{bmatrix} \lambda & 0 & 0 \\ 0 & \lambda^{-\frac{1}{2}} & 0 \\ 0 & 0 & \lambda^{-\frac{1}{2}} \end{bmatrix} \rightarrow \begin{cases} P_1 = 2\left[\frac{\partial w}{\partial I_1} + \frac{1}{\lambda}\frac{\partial w}{\partial I_2}\right]\left[\lambda - \frac{1}{\lambda^2}\right] \\ \sigma_1 = 2\left[\frac{\partial w}{\partial I_1} + \frac{1}{\lambda}\frac{\partial w}{\partial I_2}\right]\left[\lambda^2 - \frac{1}{\lambda}\right] \end{cases} \tag{16}$$

for equi-biaxial loading

$$\boldsymbol{F} = \begin{bmatrix} \lambda & 0 & 0 \\ 0 & \lambda & 0 \\ 0 & 0 & \lambda^{-2} \end{bmatrix} \rightarrow \begin{cases} P_1 = P_2 = 2\left[\frac{\partial w}{\partial I_1} + \lambda^2\frac{\partial w}{\partial I_2}\right]\left[\lambda - \frac{1}{\lambda^5}\right] \\ \sigma_1 = \sigma_2 = 2\left[\frac{\partial w}{\partial I_1} + \lambda^2\frac{\partial w}{\partial I_2}\right]\left[\lambda^2 - \frac{1}{\lambda^4}\right] \end{cases} \tag{17}$$

for pure shear loading

$$F = \begin{bmatrix} \lambda & 0 & 0 \\ 0 & 1 & 0 \\ 0 & 0 & \lambda^{-1} \end{bmatrix} \rightarrow \begin{cases} P_1 = 2\left[\frac{\partial w}{\partial I_1} + \frac{\partial w}{\partial I_2}\right]\left[\lambda - \frac{1}{\lambda^3}\right] \\ \sigma_1 = 2\left[\frac{\partial w}{\partial I_1} + \frac{\partial w}{\partial I_2}\right]\left[\lambda^2 - \frac{1}{\lambda^2}\right] \end{cases}, \tag{18}$$

for biaxial loading

$$F = \begin{bmatrix} \lambda_1 & 0 & 0 \\ 0 & \lambda_2 & 0 \\ 0 & 0 & \lambda_1^{-1}\lambda_2^{-1} \end{bmatrix} \rightarrow \begin{cases} P_1 = 2\left[\frac{\partial w}{\partial I_1} + \lambda_2^2\frac{\partial w}{\partial I_2}\right]\left[\lambda_1 - \frac{1}{\lambda_1^3\lambda_2^2}\right] \\ P_2 = 2\left[\frac{\partial w}{\partial I_1} + \lambda_2^2\frac{\partial w}{\partial I_2}\right]\left[\lambda_2 - \frac{1}{\lambda_2^3\lambda_1^2}\right] \end{cases}, \tag{19}$$

for simple shear

$$F = \begin{bmatrix} 1 & \gamma & 0 \\ 0 & 1 & 0 \\ 0 & 0 & 1 \end{bmatrix} \rightarrow P_{12} = 2\gamma\left[\frac{\partial w}{\partial I_1} + \frac{\partial w}{\partial I_2}\right],$$
$$\lambda_1 = \sqrt{1 + \frac{\gamma^2}{2} + \gamma\sqrt{1+\frac{\gamma^2}{4}}}, \tag{20}$$
$$\lambda_2 = \sqrt{1 + \frac{\gamma^2}{2} - \gamma\sqrt{1+\frac{\gamma^2}{4}}},$$

in which λ_1 and λ_2 are tension and compression eigenvalues, respectively.

Parameters estimation

In this part, the problem of finding the best model among the Tables 1, 2, 3, 4, 5, 6, to express the mechanical behaviour of a hyper-elastic material in the presence of the associated standard loading experimental data is defined in the form of an optimisation problem. Having experimental data as accuracy points, each model can be fitted to the data by finding the model's unknown parameters. On the other hand, for each model, there is no unique solution for unknown parameters and it depends on the selected estimation method. Each method achieves a set of the unknown parameter which possessing its model accuracy. Therefore, to compare the suitability of each model first of all the best and the most accurate possible form each model should be found. To this end, the well-known optimisation method namely GA is used.

The GA method is a search based method inspiring from the genetic evolution of species. In this algorithm, a population of nominated solutions to an optimisation problem is measured toward better solutions, each candidate solution has a set of properties, which can be mutated and solution are expressed in binary as strings of 0 s and 1 s [109]. The function of this algorithm is based iteration and most of its parts are selected as random processes. The cost function for the optimisation problem is the root mean square of error (RMS) of model and accuracy points as reference data. In the case of having n accuracy point,s the cost function is defined as follows:

$$\mathrm{RMS} = \sqrt{\frac{1}{\mathrm{n}} \sum_{\mathrm{i}=1}^{\mathrm{n}} \left(\tilde{\mathrm{y}}_{\mathrm{i}} - \mathrm{y}_{\mathrm{i}} \right)^2} \tag{21}$$

where, y_i is the observed value for the ith observation and $\tilde{y}_i$ is the estimated value.

The variables of the optimisation problem are the unknown parameter of each model. Having the cost function, variables, and probable constraints, the GA procedure is ready to use. Considering the flowchart depicted in Fig. 1, each step starts with defining an initial population. Then fitness of the population members (cost function for each individual) is calculated. Some genetic operators such as mutation and crossover are applied to the population to create the next generation from the previous population with more elite members. These steps are repeated to reach the stop criterion. The stop criterion is satisfied when no remarkable improvement occurs in the fitness of the population's elite members. Now let's consider the case that the constitutive mathematical model of a hyper-elastic material is required.

This model might be used in FEM software for stress analysis or used in analytical analysis. For example, experimental data of vulcanised rubber are extracted from three tests including; uniaxial tension, pure shear, and equi-biaxial

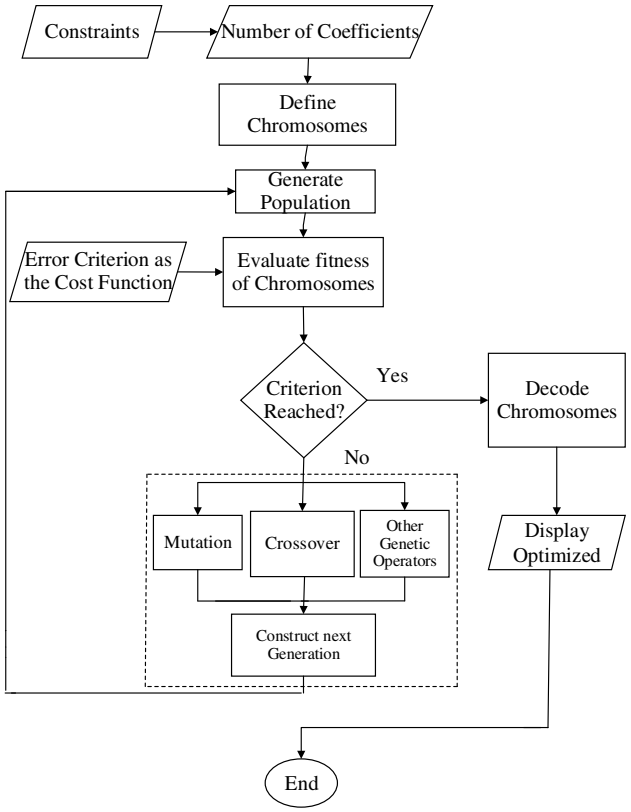

Fig. 1 The GA procedure for finding the most accurate possible form of each model

tension, and depicted by three curves in Fig. 2, Treloar [104]. Practically, working with these data raises two problems. First, there is no mathematical function for expressing stress–strain relation and second, the data do not cover the whole range of deformation, e.g. equi-biaxial and pure shear test data exist for a range of stretch from 1 to 4.5 while for the uniaxial test from 1 to 7. That is why using the constitutive models of Tables 1, 2, 3, 4, 5, 6 is inevitable in applications. Using Tables 1, 2, 3, 4, 5, 6 and the proposed GA, the best possible model's unknown parameters for predicting the uniaxial loading of Treloar [104] data are summarised in Table 7. Also, the best possible function for each model is depicted in Fig. 3. Both Table 7 and Fig. 3 shows that Swanson model is the most accurate model for predicting the uniaxial behaviour of this set of reference data. The Fig. 3 shows the Neo–Hookean and Gent–Thomas have the worst accuracy for uniaxial loading. Another study of Treloar [104] is related to the pure shear loading data. When the pure shear loading data are assumed as the reference data, it is concluded from Table 8, and Fig. 4 that the model Carrol has the most accuracy while Neo–Hookean has the worst.

Table 9 and Fig. 5 summarise the result obtaining form finding the best possible model fitted on the equi-biaxial

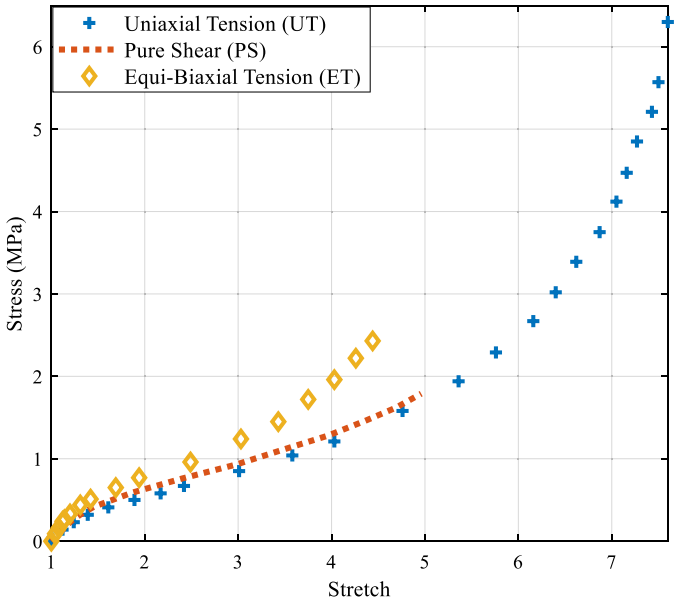

Fig. 2 Experimental data of vulcanised rubber containing 8% sulphur [104]

Table 7 Evaluated parameters of models with uniaxial tension test data

Model	Parameters				*R*-square
Neo–Hookean	$\mu = 0.5672MPa$				0.8363
Mooney–Rivlin	$C_{10} = 0.4064MPa$		$C_{01} = -0.7476MPa$		0.8977
Isihara	$C_{10} = 0.1152MPa$	$C_{20} = 0.0001814MPa$		$C_{01} = 0.8642MPa$	0.9922
Gent–Thomas	$C_1 = 0.2754MPa$		$C_2 = 2.81 \times 10^{-11}MPa$		0.8265
Swanson	$A_1 = 4.27 \times 10^{-5}$		$B_1 = 0.3813$		0.9990
	$\alpha_1 = 3.884$		$\beta_1 = 1.218$		
Yeoh	$C_1 = 0.1627$	$C_2 = -0.001161$		$C_3 = 3.734 \times 10^{-5}$	0.9987
Arruda–Boyce	$\mu = 0.2313MPa$		$N = 19.38$		0.9963
Gent	$\mu = 0.251379MPa$		$J_m = 81.16$		0.8688
Carrol	$a = 0.1679MPa, b = 1.533 \times 10^{-6}MPa$ $c = 0.01307MPa$				0.9498
Ogden	$\mu_1 = 0.0391$	$\mu_2 = 0.0171$		$\mu_3 = 0.0164$	0.9719
	$\alpha_1 = 2.344$	$\alpha_2 = 3.772$		$\alpha_3 = 0.0327$	
3-Chain	$\mu = 0.2596$		$N = 76.31$		0.9987
8-Chain	$\mu = 0.2893$		$N = 24.32$		0.9411

loading data from Treloar [104]. It is seen that Ogden is the most suitable model for prediction of mechanical behaviour of the specimen under the equi-biaxial loading, while Isihara and Neo–Hookean have the worst accuracy. From Eqs. 16 to 20, it is clear that each constitutive model has different parameters and different mathematical functions for different loadings, e.g. for three types of loading, three functions for the 3-chain model are obtained as follows:

$$\sigma_{\mathrm{UT}} = \frac{\mu}{3}\left(\frac{3\lambda N - \lambda^3}{N - \lambda^2} - \lambda^{-2}\frac{3N - \lambda^{-1}}{N - \lambda^{-1}}\right),$$

$$\mu = 0.2596, N = 76.31, \tag{22}$$

$$\sigma_{\mathrm{ET}} = \frac{\mu}{3}\left(\frac{2\lambda N - \lambda^3}{N - \lambda^2} - \lambda^{-5}\frac{3N - \lambda^{-4}}{N - \lambda^{-4}}\right),$$

$$\mu = 0.3126, N = 154.4, \tag{23}$$

$$\sigma_{\mathrm{PS}} = \frac{\mu}{3}\left(\frac{3\lambda N - \lambda^3}{N - \lambda^2} - \lambda^{-3}\frac{3N - \lambda^{-2}}{N - \lambda^{-2}}\right),$$

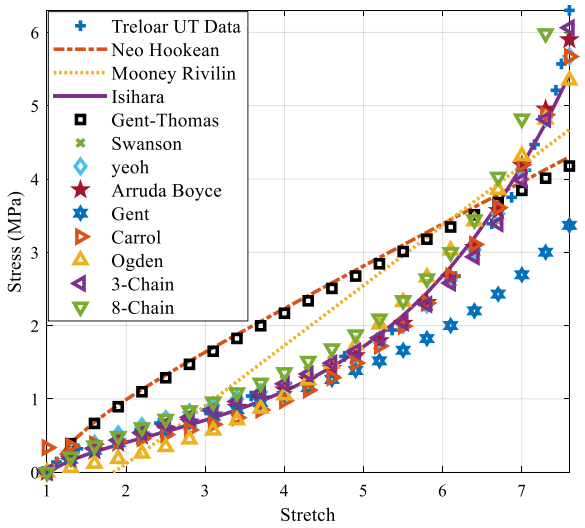

Fig. 3 The best accurate function of each model for uniaxial loading

$$\mu = 0.4269, N = 165.41, \tag{24}$$

As it is depicted in Figs. 3, 4, 5, three functions of Eqs. 22 to 24 accurately describe the mechanical behaviours of the 8% Sulphur vulcanised rubber of Fig. 2. In spite of the accurate description of each type of loading test data by of these three functions, no one can describe the whole mechanical behaviour completely. To obtain a unique function which, not only be based on 3-chain model but also can relatively describe whole data of Fig. 2 let's consider function σ_o similar to one of the functions in Eqs. 22 to 24 e.g. Equation 22. This function's parameters again are determined using GA; however, this time the cost function is defined such that the data of the three types of loading is considered as the reference or accuracy points. Defining the cost function as follows:

$$\begin{aligned} \mathrm{CF} = {} & W_1 \sqrt{\frac{1}{n_1}\sum_{i=1}^{n1}\left(\tilde{y}_{\mathrm{UTi}} - y_i\right)}^2 + W_2 \sqrt{\frac{1}{n_2}\sum_{i=1}^{n_2}\left(\tilde{y}_{\mathrm{ETi}} - y_i\right)}^2 \\ & + W_3 \sqrt{\frac{1}{n_3}\sum_{i=1}^{n_3}\left(\tilde{y}_{\mathrm{PSi}} - y_i\right)}^2 \end{aligned} \tag{25}$$

where CF is overall cost function, W_1–W_3 are weight of each single cost function that show the relative importance of each single cost function among the overall cost function, n_1–n_3 are number of reference data in each type of loading, and $\tilde{y}_{\mathrm{UTi}}$, $\tilde{y}_{\mathrm{ETi}}$ and $\tilde{y}_{\mathrm{PSi}}$ are reference or accuracy points of each type of loading test data. After optimise the function σ_{UT} with respect to the cost function 25 the parameters μ and N are obtained as follows:

$$\mu = 0.3329, N = 87.91. \tag{26}$$

The new optimised σ_{o} function is depicted in Fig. 6.

It is seen that the function is slightly distant from each reference data such that it is placed between them. This function obtained using $W_1 = 1$, $W_2 = 1$ and $W_3 = 2$. Selecting another set of W_i's, the function approaches to the associated reference data with largerW_i. For M type of loading the cost function can be generally defined as follows:

$$\mathrm{CF} = \sum_{j=1}^{M}\left[W_j \sqrt{\frac{1}{n_j}\sum_{i=1}^{n_j}\left(\tilde{y}_{ji} - y_i\right)^2}\right], \tag{27}$$

Table 8 Evaluated parameters of models with pure shear test data

Model	Parameters				*R*-Square
Neo–Hookean	$\mu = 0.3347MPa$				0.9950
Mooney–Rivlin	$C_{10} = -24.63$		$C_{01} = 24.8$		0.9943
Isihara	$C_{10} = 0.16MPa$	$C_{20} = 0.0037MPa$		$C_{01} = 0.003MPa$	0.9970
Gent–Thomas	$C_1 = 0.1709MPa$		$C_2 = -0.01837MPa$		0.9940
Swanson	$A_1 = -9$		$B_1 = 9.324$		0.9943
	$\alpha_1 = 0.1459$		$\beta_1 = 0.1423$		
Yeoh	$C_1 = 0.1765$	$C_2 = -0.001548$		$C_3 = 4.879 \times 10^{-5}$	0.9995
Arruda–Boyce	$\mu = 0.3106MPa$		$N = 45.56$		0.9965
Gent	$\mu = 0.3393MPa$		$J_m = -1.638 \times 10^6$		0.9939
Carrol	$a = 0.1307MPa$ $b = 4.862 \times 10^{-7}MPa$ $c = 0.1798MPa$				0.9997
Ogden	$\mu_1 = 0.304$	$\mu_2 = 0.036$		$\mu_3 = 0.849$	0.9949
	$\alpha_1 = 2.079$	$\alpha_2 = 0.959$		$\alpha_3 = 0.655$	
3-Chain	$\mu = 0.3126$		$N = 154.4$		0.9954
8-Chain	$\mu = 1.025$		$N = 0.01673$		0.9940

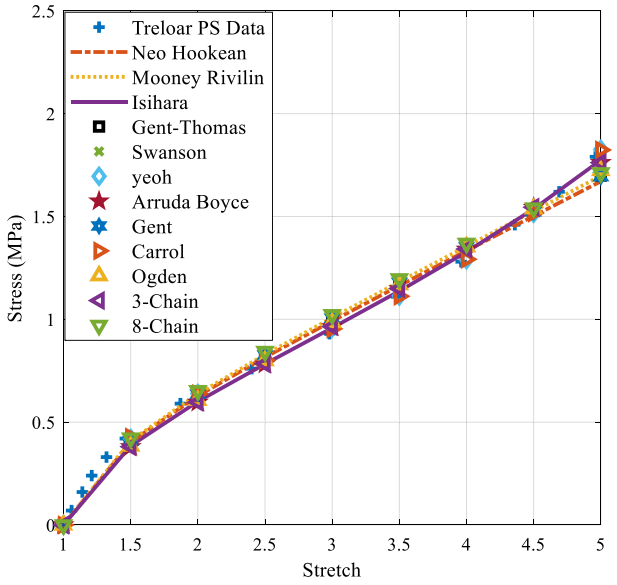

Fig. 4 The best accurate function of each model for pure shear loading

in which $\tilde{y}_{ji}$ is i th accuracy point of loading test data j th, and n_j is number of data of test data j th.

Conclusion

In this research, 50 constitutive models of hyper-elastic materials are collected and classified into the six categories including; polynomial function of the first invariant, the polynomial function of first and second invariants, functions of first and second invariants, functions of principal tensions of deformation gradient tensor, functions of combinations of principal tensions of deformation gradient tensor and first and second invariants, and models based on chemical structures and quasi-rubber material network. The mathematical function of each model is not unique and depends on the type of loading, physical parameters, Cauchy stress tensor, hydrosstatic pressure, and nominal stress. Five standard loadings were introduced including; uniaxial, equi-biaxial, pure shear, biaxial, and simple shear loading. The physical parameters were taken into account for each type of loading. It was presented how to determine the most possible accurate unknown parameters of each model using GA, when experimental test data exist. Also, it was shown that using this algorithm and using a combinational cost function, all types of loading test data can be explained by an approximate unique function.

Table 9 Evaluated parameters of models with equi-biaxial tension test data

Model	Parameters				*R*-square
Neo–Hookean	$\mu = 0.4729$ MPa				0.9685
Mooney–Rivlin	$C_{10} = 0.1713$ MPa		$C_{01} = 0.004685$ MPa		0.9952
Isihara	$C_{10} = 0.199$ MPa	$C_{20} = 0.0015$ MPa		$C_{01} = 0.0013$ MPa	0.9224
Gent–Thomas	$C_1 = 0.2559$ MPa		$C_2 = -0.1965$ MPa		0.9802
Swanson	$A_1 = 0.3275$		$B_1 = 0.002204$		0.9917
	$\alpha_1 = 0.199$		$\beta_1 = 0.0015$		
Yeoh	$C_1 = 0.2037$	$C_2 = -0.001295$		$C_3 = 0.0001314$	0.9997
Arruda–Boyce	$\mu = 0.3531$ MPa		N = 13.76		0.9980
Gent	$\mu = 0.36401$ MPa		$J_m = 111.899$		0.9973
Carrol	$a = 0.2489$ MPa $b = 3.213 \times 10^{-7}$ MPa $c = -0.1029$ MPa				0.9997
Ogden	$\mu_1 = 0.05454$	$\mu_2 = 0.07876$		$\mu_3 = 1.906$	0.9998
	$\alpha_1 = -1.971$	$\alpha_2 = 3.935$		$\alpha_3 = 0.3266$	
3-Chain	$\mu = 0.4269$		$N = 165.41$		0.9963
8-Chain	$\mu = 1.241$		$N = 0.007901$		0.9951

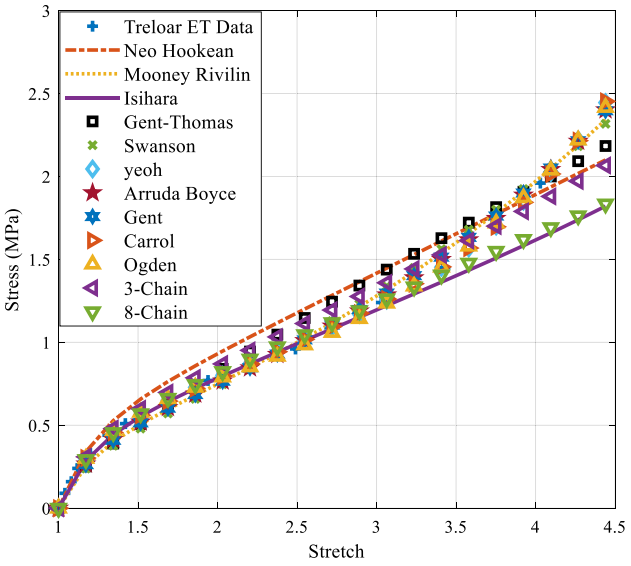

Fig. 5 Comparison between models and equi-biaxial experiment data

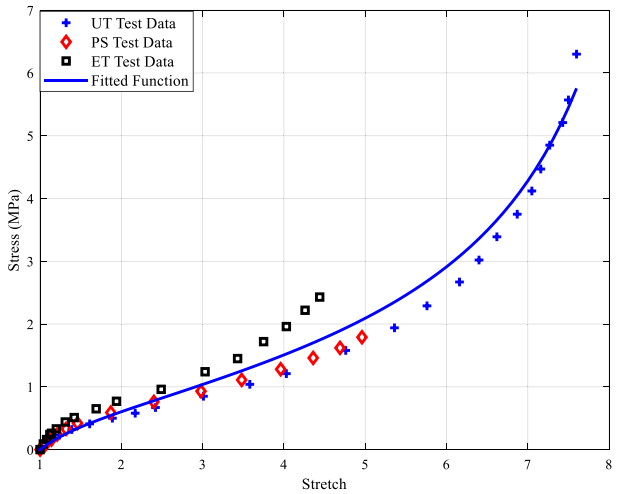

Fig. 6 A unique function to be relatively close to the three types of loading test data

Conflict of interest

On behalf of all authors, the corresponding author states that there is no conflict of interest.

References

1. Mc Allen J, Cuitino AM, Sernas V (1996) Numerical investigation of the deformation characteristics and heat generation in pneumatic aircraft tires part i-mechanical modeling. Finite Elem Anal Des 23:241–263
2. Mc Allen J, Cuitino AM, Sernas V (1996) Numerical investigation of the deformation characteristics and heat generation in pneumatic aircraft tires part ii-thermal modeling. Finite Elem Anal Des 23:265–290
3. Lin YJ, Hwang SJ (2004) Temperature prediction of rolling tire by computer simulation. Math Comput Simul 67:235–249
4. Luo R, Mortel W, Wu X (2015) Investigation on rubber failure due to heat generation under dynamic loading. Proc Inst Mech Eng Part L J Mater Design Appl 229:77–87
5. Rafei M, Ghoreishy MHR, Naderi G (2018) Thermo-mechanical coupled finite element simulation of tire cornering characteristics-effect of complex material models and friction law. Math Comput Simul 144:35–51
6. Banic M, Stamenkovic DV, Miltenovic V, Milosevic M, Miltenovic A, Djekic P, Rackov M (2012) Prediction of heat generation prediction in rubber or rubber-metal springs. Thermal Sci 16:527–539
7. Banic M, Miltenovic V, Milosevic M, Miltenovic A, Jovanovic N (2012) heat generation prediction in the rail way draw gear rubber-metal spring. Facta Univ Ser Mech Eng 10:171–180
8. Luo Y, Liu Y, Yin HP (2013) Numerical investigation of nonlinear properties of a rubber absorber in rail fastening systems. Int J Mech Sci 69:107–113
9. Han C, Zhang J, Liang Zh (2014) Thermal failure of rubber bushing of a positive displacement motor: a study based on thermo-mechanical coupling. Appl Therm Eng 67:489–493
10. Rastgoo Moghadam S, Konstantinidis D (2017) Finite element study of the effect of support rotation on the horizontal behavior of elastomeric bearings. Compos Struct 163:474–490
11. Paetsch C, Trimmer BA, Dorfmann A (2012) A constitutive model for active-passive transition of muscle fibers. Int J Non Linear Mech 47:377–384
12. Ehret AE, Bol M, Itskov M (2011) A continuum constitutive model for the active behaviour of skeletal muscle. Mech Phys Sol 59:625–636
13. Natali AN, Fontanella CG, Carniel EL (2010) Constitutive formulation and analysis of heel pad tissues mechanics. Med Eng Phys 32:516–522
14. Cabrera MS, Oomens CWJ, Bouten CVC, Bogers AJJC, Hoerstrup SP, Baaijens FPT (2013) Mechanical analysis of ovine and pediatric pulmonary artery for heart valve stent design. J Biomech 46:2075–2081
15. Taha Z, Norman MS, Syed Omar SF, Suwarganda E (2016) A finite element analysis of a human foot model to simulate neutral standing on ground. Procedia Eng 147:240–245
16. Cornin DS, Singh D, Gierczycka D, Barker J, Shen D (2018) Modeling the neck for impact scenarios. Basic Finite Elem Method Appl Injury Biomech Chap 13:503–538
17. Shearer T (2015) A new strain energy function for hyper-elastic modeling of ligaments and tendons based on fascicle microstructure. J Biomech 48:290–297
18. Swedberg AM, Reese SP, Maas SA, Ellis BJ, Weiss JA (2014) Continuum description of the poisson's ratio of ligaments and tendon under finite deformation. J Biomech 47:3201–3209
19. Huang H, Tang W, Yan B, Wu B (2012) Mechanical response of periodontal ligament under a realistic orthodontic loading. Procedia Eng 31:828–833
20. Morales-Orcajo E, Souza TR, Bayod J, De Las CRB, (2017) Non-linear finite element model to assess the effect of tendon forces on the foot-ankle complex. Med Eng Phys 49:71–78
21. Mahmu J, Holt C, Evans S, Manan NFA, Chizari M (2012) A parametric study and simulations in quantifying human skin hyper-elastic parameters. Procedia Eng 41:1580–1586
22. Nolan DR, Gower AL, Destrade M, Ogden RW, McGarry JP (2014) A robust anisotropic hyper-elastic formulation for the modeling of soft tissue. J Mech Behav Biomed Mater 39:48–60

23. Bergstom JS, Boyce MC (2001) Constitutive modeling of time-dependent and cycle loading of elastomers and application to soft biological tissues. Mech Mater 33:523–530
24. Abbasi AA, Ahmadian MT (2012) Large deformation characterization of mouse oocyte cell under needle injection experiment. AUT J Model Simulat 44(1):21–25
25. McBride A, Bargmann S, Pond D, Limbert G (2016) Thermoelastic modeling of the skin at finite deformation. J Therm Biol 62:201–209
26. Caro-Bretelle AS, Ienny P, Leger R, Corn S, Bazin I, Bretelle F (2016) Constitutive modeling of stress softening and permanent set in a porcine skin tissue: impact of the storage preservation. J Biomech 49:2863–2869
27. Mendizabal A, Aguinaga I, Sanchez E (2015) Characterization and modeling of brain tissue for surgical simulation. J Mech Behav Biomed Mater 45:1–10
28. Miller K, Chinzei K (2002) Mechanical properties of brain tissue in tension. J Biomech 35:483–490
29. Budday S, Sommer G, Birkl C, Langkammer C, Haybaeck J, Kohnert J, Bauer M, Paulsen F, Steinmann P, Kuhl E, Holzapfel GA (2017) Mechanical characterization of human brain tissue. Acta Biomater 45:319–340
30. Mihai LA, Budday S, Holzapfel GA, Kuhl E, Goriely A (2017) A family of hyper-elastic models for human brain tissue. J Mech Phys Sol 106:60–79
31. Cardoso C, Fernandes CS, Lima R, Ribeiro J (2018) Biomechanical analysis of PDMS channels using different hyper-elastic numerical constitutive models. Mech Res Commun 90:26–33
32. Voyiadjis GC, Samadi-Dooki A (2018) Hyper-elastic modeling of the human brain tissue: effects of no-slip boundary condition and compressibility on the uniaxial deformation. J Mech Behav Biomed Mater 83:63–78
33. Ramirez-Torres A, Rodriguez-Ramos R, Merodio J, Bravo-Castillero J, Guinovart-Diaz R, Alfonso JCL (2015) Action of body forces in tumor growth. Int J Eng Sci 89:18–34
34. Beccani M, Di Natali C, Hall NE, Benjamin CE, Bell CS, Valdastri P (2014) Wireless tissue palpation: characterization of the probe head to improve detection of tumors in soft tissue. Proceida Eng 87:352–355
35. Zaeimdar S (2014) Mechanical characterization of breast tissue constituents for cancer assessment, the degree of master of applied science, School of Mechatronic Systems Engineering, Faculty of Applied science, Simon Fraser University, Spring.
36. Lyne S, Wang Z, Nicolini LF, Mosadegh B, Whitesides GM, Walsh CJ (2013) Towards a soft pneumatic glove for hand rehabilitation. In: International Conference On Intelligent Robots and Systems, Tokyo, Japan, pp 1512–1518.
37. Barani Z, Haghpanahi M, Katozian H, Saeidi H (2013) A three dimensional stress analysis of diabetic insol and evaluation of silicone gel material using finite element approach. In: International Conference On Intelligent Robots and Systems, Tokyo, Japan, pp 1512–1518.
38. Matsuda A, Tanabe H, Nagaoka T, Nakashima M, Shimana T, Omori K (2013) 3D-CG based stress calculation of competitive swimwear using anisotropic hyper-elastic model. Proceida Eng 60:349–354
39. Shimana T, Nakashima M, Matsuda A, Omori K (2013) A new method for designing sportswear by using three dimensional computer graphic based anisotropic hyper-elastic models and musculoskeletal simulations. Proceida Eng 60:331–336
40. Tanabe H, Matsuda A, Shimana T, Omori K (2012) Numerical analysis of competitive swimwear using finite element method. Proceida Eng 34:718–723
41. Burbank SD, Smith LV (2012) Dynamic characterization of rigid foam used in finite element sports ball simulations. J Sports Eng Technol 226(2):77–85
42. Munroe BJ, Sherwood JA (2012) Finite element modeling of a baseball. Proceida Engineering 34:610–615
43. Andena L, Briatico-Vagosa F, Ciancio A, Pavan A (2014) A finite element model for the prediction of force reduction of athletics tracks. Proceida Eng 72:847–852
44. Allen T, Hart J, Spurr J, Haake S, Goodwill S (2010) Validated dynamic analysis of real sports equipment using finite element; a case study using tennis rackets. Proceida Eng 2:3275–3280
45. Payne T, Mitchel S, Bibb R, Waters M (2015) Development of novel synthetic muscle tissues for sport impact surrogates. J Mech Behav Biomed Mater 41:357–374
46. Tanaka K, Teranishi Y, Ujihashi S (2010) Experimental and finite element analyses of a golf ball colliding with a simplified club during a two dimensional swing. Proceida Eng 2:3249–3254
47. Pang TY, Subic A, Takla M (2011) Finite element analysis of impact between cricket ball and cantilever beam. Proceida Eng 13:258–264
48. Ranga D, Strangwood M (2010) Finite element modeling of the quasi-static and dynamic behaviour of a solid sports ball based on component material properties. Proceida Eng 2:3287–3292
49. Nevins D, Smith L (2014) Head impact response to simulated ball-to-head collisions. Proceida Eng 72:545–500
50. Rinaldi RG, Manin L, Bonnard C, Drillon A, Lourenco H, Havard N (2016) Non linearity of the ball/rubber impact in table tennis: experiments and modeling. Proceida Eng 147:348–353
51. Mooney M (1940) A theory of large elastic deformation. J Appl Phys 11:582–592
52. Kuhn W, Grun F (1942) Beziehungen zwischen elastischen konstanten und dehnungsdoppeldbrechung hochelastischer stoffe. Kolloid-Zeitschrift 101(3):248–271
53. Treloar LRG (1943) The elasticity of a network of long-chain molecules I. J Trans Faraday Soc 39:36–41
54. Rivlin RS, Saunders DW (1951) Large elastic deformation of isotropic materials. vii. experiments on the deformation of rubber. J Philos Trans R Soc Lond 243:251–288
55. Isihara A, Hashitsume N, Tatibana M (1951) Statistical theory of rubber-like elasticity, part IV. J Chem Phys 19(12):1508–1512
56. Hart-Smith LJ (1966) Elasticity parameters for finite deformations of rubber-like materials. J Zeitschrift Fur Angewandte Mathematik Und Physik ZAMP 17(5):608–626
57. Fung YCB (1967) Elasticity of soft tissues in sample elongation. Am J Physiol 213(6):1532–1544
58. Alexander H (1968) A constitutive relation for rubber-like materials. Int J Eng Sci 213(9):549–563
59. Ball RC, Doi M, Edwards SF, Warnert M (1981) Elasticity of entangled networks. Polymer 22:1010–1018
60. Flory JF, Erman B (1982) Theory of elasticity of polymer network 3. Macromolecules 15(3):800–806
61. Kilian HG, Enderle HF, Unseld K (1986) The use of the van der waals model to elucidate universal aspects of structure-property relationships in simply extended dry and swollen rubbers. J Coll Polym Sci 264:866–876
62. Gao YC (1997) Large deformation field near a crack tip in rubber-like material. Theoret Appl Fract Mech 26(11–12):155–162
63. Shariff MHBM (2000) Strain energy function for filled and unfilled rubberlike material. Rubber Chem Technol 73:1–18
64. Pucci E, Saccomandi G (2002) A note on the gent model for rubber-like materials. Rubber Chem Technol 75(5):839–851
65. Beda T, Chevalier Y (2003) Hybrid continuum model for large elastic deformation of rubber. J Appl Phys 94(4):2701–2706
66. Nunes LCS (2011) Mechanical characterization of hyper-elastic polydimethylsiloxane by simple shear test. Mater Sci Eng, A 528(3):1799–1804

67. Khajehsaeid H, Arghavani J, Naghdabadi R (2013) A hyper-elasticity constitutive model for rubber-like materials. Eur J Mech A/Sol 38:144–151
68. Yokota T, Gen M, Li Y-X (1996) Genetic algorithm for nonlinear mixed integer programming problems and its applications. Comput Ind Eng 30:905–917
69. Mitsuo Gen RC (2000) Genetic algorithms and engineering design. Wiley, New York
70. Sadeghi J, Sadeghi S, Niaki STA (2014) Optimizing a hybrid vendor-managed inventory and transportation problem with fuzzy demand: an improved particle swarm optimization algorithm. Inf Sci 272:126–144
71. Rivlin RS (1948) Large elastic deformation of isotropic materials. i. fundamental concepts. J Philos Trans R Soc Lond 240(822):459–490
72. Ogden RW (1972) 'Large deformation isotropic elasticity on the correlation of theory and experiment for incompressible rubber-like solids In: Proceedings of the Royal Society of London. A. Mathematical and Physical Sciences, Vol. 326, pp. 565–84
73. Ogden RW (1984) Nonlinear elastic deformation, England. Ellis Harwood, Chichester
74. Yeoh OH (1990) Characterization of elastic properties of carbon-black-filled rubber vulcanizates. Rubber Chem Technol 63(5):792–805
75. Arruda EM, Boyce MC (1993) A three-dimensional constitutive model for the large stretch behavior of rubber elastic materials. J Mech Phys Sol 41(2):389–412
76. Beda T (2014) An approach for hyper-elastic model-building and parameters estimation a review of constitutive models. Eur Polymer J 50:97–108
77. Gent AN (1996) A new constitutive relation for rubber. Rubber Chem Technol 69(5):59–61
78. Lopez-Pamies O (2010) A New I1-based hyper-elastic model for rubber elastic materials. CR Mec 338(1):3–11
79. Hesebeck O, Wulf A (2018) Hyper-elastic constitutive modeling with exponential decay and application to a viscoelastic adhesive. Int J Sol Struct 141:60–72
80. Biderman VL (1958) Calculation of rubber parts (In Russian). Rascheti Na Prochnost, Moscow
81. Tschoegl NW (1971) Constitutive equations for elastomers. J Polym Sci Part A 1 9:1959–1970
82. James AG, Green A, Simpson GM (1975) Strain energy functions of rubber. i, characterization of gum vulcanizates. J Appl Polym Sci 19:2033–2058
83. Swanson SR (1985) A constitutive model for high elongation elastic materials. J Eng Mater Technol 107:110–114
84. Lion A (1997) On the large deformation behaviour of reinforced rubber at different temperatures. J Mech Phys Solids 45(11–12):1805–1834
85. Haupt P, Sedlan K (2001) ViscoPlasticity of elastomeric materials: experimental facts and constitutive modeling. Arch Appl Mech 71(2-3):89–109
86. Beda T (2005) Reconciling the fundamental phenomenological expression of the strain energy of rubber with established experimental facts. J Polym Sci Part B 43(2):125–134
87. Amin AFMS, Wiraguna SI, Bhuiyan AR, Okui Y (2006) Hyper-elasticity model for finite element analysis of nature and high damping rubbers in compression and shear. J Eng Mech 132:54–64
88. Carroll MM (2011) A strain energy function for vulcanized rubbers. J Elast 103(2):1713–1732
89. Gent AN, Thomas AG (1958) Forms for the stored (strain) energy function for vulcanized rubber. J Polym Sci 28(118):625–628
90. Veronda DR, Westmann RA (1958) Mechanical characterization of skin-finite deformations. J Biomech 3(1):111–124
91. Takamizawa K, Hayashi K (1987) Strain energy density function and uniform strain hypothesis for arterial mechanics. J Biomech 20(1):7–17
92. Holmes MH, Mow VC (1990) The nonlinear characteristics of soft gels and hydrated connective tissues in ultrafiltration. J Biomech 23(11):1145–1156
93. Yeoh OH, Fleming PD (1997) A new attempt to reconcile the statistical and phenomenological theories of rubber elasticity. J Polym Sci Part B 35(12):1919–1931
94. Lambert-Diani J, Rey C (1999) New phenomenological behavior laws for rubbers and thermoplastic elastomers. Eur J Mech A/Solids 18(6):1027–1043
95. Beda T (2007) Modeling hyper-elastic behavior of rubber: a novel invariant-based and a review of constitutive models. J Polym Sci Part B 45(2):1713–1732
96. Valanis KC, Landel RF (1967) The stain energy function of a hyper-elastic material in terms of the extension ratios. J Appl Phys 38:2997–3002
97. Peng STJ, Landel RF (1972) Stored energy function of rubber like materials divided from simple tensile data. J Appl Phys 43:3063–3067
98. Tobisch K (1980) Contribution to the mathematical description of stress-strain on behavior of elastomers. J Rub Technol 53:836–841
99. Narooei K, Arman M (2018) Generalization of exponential based hyper-elastic to hyper-viscoelastic model for investigation of mechanical behavior of rate dependent materials". J Mech Behav Biomed Mater 79:104–113
100. Heinrich G, Kaliske M (1997) Theoretical and numerical formulation of a molecular based constitutive tube-model of rubber elasticity. J Comput Theor Polym Sci 7(3/4):227–241
101. Heinrich G, Kaliske M (1999) An extended tube-model for rubber elasticity: statistical-mechanical theory and finite element implementation. Rubber Chem Technol 72:602–632
102. Shahzad M, Kamran A, Siddiqui MZ, Farhan M (2015) Mechanical characterization and FE modeling of a hyper-elastic material. Mater Res 18:918–924
103. Wu Y, Wang H, Li A (2006) Parameter identification methods for hyper-elastic and hyper-visoelastic models. Appl Sci 6:01–13
104. Treloar LRG (1944) Stress–strain data for vulcanized rubber under types of deformation. J Trans Faraday Soc 40:59–70
105. Lee SB, Rivin EI (1996) Finite element analysis of load-deflection and creep chracteristics of compressed rubber components for vibration control devices. J Mech Design 118:328–336
106. Breslavsky I, Amabili M, Legrand M (2014) Nonlinear vibrations of thin hyperelastic plates. J Sound Vib 333:4668–4681
107. Budday S, Sommer G, Birkl C, Langkammer C, Haybaeck J, Kohnert J, Bauer M, Paulsen F, Steinmann P, Kuhl E, Holzapfel GA (2017) Mechanical characterization of human brain tissue. Acta Biomater 48:319–340
108. Diani J, Brieu M, Vacherand JM, Rezgui A (2004) Directional model for isotropic and anisotropic hyper-elastic rubber-likr materials. Mech Mater 36:313–321
109. Whitley D (1994) A genetic algorithm tutorial. Stat Comput 4:65–85